DISEASES AND DISORDERS

Atrophy associated with tau pathology precedes overt cell death in a mouse model of progressive tauopathy

Christine W. Fung[1,2]*, Jia Guo[3,4]*, Hongjun Fu[5], Helen Y. Figueroa[1,6], Elisa E. Konofagou[2], Karen E. Duff[1,6,7]†

Tau pathology in Alzheimer's disease (AD) first develops in the entorhinal cortex (EC), then spreads to the hippocampus, followed by the neocortex. Overall, tau pathology correlates well with neurodegeneration and cell loss, but the spatial and temporal association between tau pathology and overt volume loss (atrophy) associated with structural changes or cell loss is unclear. Using in vivo magnetic resonance imaging (MRI) with tensor-based morphometry (TBM), we mapped the spatiotemporal pattern of structural changes in a mouse model of AD-like progressive tauopathy. A novel, coregistered in vivo MRI atlas was then applied to identify regions in the medial temporal lobe that had a significant volume reduction. Our study shows that in a mouse model of tauopathy spread, the propagation of tau pathology from the EC to the hippocampus is associated with TBM-related atrophy, but atrophy in the dentate gyrus and subiculum precedes overt cell loss.

INTRODUCTION

One of the major pathological hallmarks of Alzheimer's disease (AD) and the primary tauopathies that cause frontotemporal degeneration (FTD-tau) is the accumulation of insoluble, hyperphosphorylated tau protein into intraneuronal neurofibrillary tangles (NFTs), threads, and inclusions (*1*). In healthy neurons, the tau protein stabilizes axonal microtubules that are necessary for proper neuronal function (*2*). In AD and the tauopathies, the abnormal accumulation of tau protein in somatodendritic compartments is associated with axonal and synaptic dysfunction, cerebral atrophy, neuronal loss, and ultimately, clinical and functional decline (*1*, *3*, *4*). In the earliest stages of AD, tauopathy begins in the entorhinal cortex (EC). It then develops in the hippocampus and neocortical areas at later stages, which correlates with cognitive impairment (*1*). However, it is not yet fully understood how, and to what extent, the progressive spread of tau pathology is associated with axonal and synaptic dysfunction and its relationship with cerebral atrophy and neuronal loss over time.

Imaging techniques such as positron emission topography (PET) and magnetic resonance imaging (MRI) have been used to explore the relationship between the distribution of tau pathology and atrophy, respectively, in human AD (*5*–*13*). However, tau PET ligands have only recently been applied in human AD, and longitudinal studies are limited. As human AD is characterized by the accumulation of amyloid plaques and tau NFTs, the impact of tau pathology per se on degeneration is unclear. To address this, a line of transgenic tau mice (line EC-Tau) that expresses an aggregating form of human tau at relatively high levels in the hippocampal formation was used to investigate the spatial and temporal spread of tauopathy and its role in pathogenesis (*14*, *15*). Previous studies in this and similar mouse lines have shown that tau pathology originating in the EC can spread transynaptically from regions of primary vulnerability to secondary affected areas along neuroanatomically connected routes (*14*–*16*), and the idea that tauopathy spreads through the brain has gained credibility. However, it has not been demonstrated that pathology spread is accompanied by neurodegeneration in secondary affected regions, and the temporal and spatial relationship between pathology and neurodegeneration in models of progressive spread of tauopathy has yet to be shown.

Our aim was to elucidate the relationship between the spread of pathological tau and the associated spread of atrophy (volume reduction). To do this, we used EC-Tau mice at 20 to 24 months old (which represents an early stage in human AD tauopathy) and another group of EC-Tau mice at 30 to 36 months old (which represents a moderate stage) and compared them with their age-matched littermates (controls). Tau pathology in EC-Tau mice at the early stage is mainly observed in the EC (*16*). By the moderate stage, tau protein has spread and accumulated in cell bodies throughout the hippocampal formation, and significant neuronal loss in the EC and pre-/para-subiculum (PPS) is seen (*15*).

We used tensor-based morphometry (TBM) with MRI to observe the global and regional structural changes between the EC-Tau mice and their age-matched controls at the early and moderate stages. TBM is an imaging technique used to localize regions of shape differences based on nonlinear deformation fields that align, or warp, images to a common anatomical template (*17*). The Jacobian map is the determinant of the Jacobian matrix of a deformation field and quantifies the local change in volume at the voxel level to evaluate whether a volume loss (or growth) has occurred. In this study, we not only show that atrophy spreads from the EC to the hippocampus alongside tau pathology, but we also identify areas in the hippocampus with atrophy at the later stage that showed no change in the number of $NeuN^+$ neurons in ex vivo studies. In addition, we visualized the spread of atrophy and tau pathology in three-dimensional (3D) reconstructed images and were able to demonstrate that the spread of tau pathology is associated with significant TBM-related reductions in volume but precedes overt cell loss at the moderate stage.

[1]Taub Institute for Research on Alzheimer's Disease and the Aging Brain, Columbia University, 630 West 168th Street, New York, NY 10032, USA. [2]Department of Biomedical Engineering, Columbia University, 500 W 120th Street, New York, NY 10025, USA. [3]Department of Psychiatry, Columbia University, 1051 Riverside Drive, New York, NY 10032, USA. [4]Zuckerman Institute, Columbia University, 3227 Broadway, New York, NY 10027, USA. [5]Department of Neuroscience, Chronic Brain Injury, Discovery Themes, The Ohio State University, Columbus, OH 43210, USA. [6]Department of Pathology and Cell Biology, Columbia University, 630 West 168th Street, New York, NY 10032, USA. [7]UK Dementia Research Institute at University College London, London, UK.
*These authors contributed equally to this work.
†Corresponding author. Email: k.duff@ucl.ac.uk

RESULTS

Significant volume reduction in the MTL of EC-Tau mice

We used EC-Tau mice at 20 to 24 months old (early stage, $n = 11$) and another group of EC-Tau mice at 30 to 36 months old (moderate stage, $n = 10$) and compared each group with their age-matched littermates (controls; early stage $n = 10$, moderate stage $n = 10$). Voxel-based analyses were performed to determine the amount of significant volume reduction (atrophy) in the EC-Tau group compared with their age-matched control group. Figure 1 shows a schematic of the timeline of the MRI image acquisition and image processing pipeline. A 3D rendering of the mouse brain was generated using 3DSlicer software. An in vivo MRI mouse atlas (*18*) was used to locate different subregions in the mouse brain, specifically the cortex and hippocampus. In our analyses, we focused on significant atrophy in the medial temporal lobe (MTL). The MTL consists of the EC [medial EC (MEC) and lateral EC (LEC)] and the hippocampus [dentate gyrus (DG); cornu ammonis, CA1, CA2, and CA3; and dorsal hippocampal commissure (dhc)], which includes the subicular complex [subiculum (Sub) and post-Sub (Post)].

Our analyses showed that at the early stage, significant volume reduction was observed in the EC of the EC-Tau mice ($n = 11$, mean age = 20.71 months) compared with their controls ($n = 10$, mean age = 20.70 months) (Fig. 2A). At the moderate stage, the atrophy in the EC had spread to other regions in the MTL in the EC-Tau mice ($n = 10$, mean age = 33.38 months) compared with their control group ($n = 10$, mean age = 32.26 months) (Fig. 2B). More specifically, this significant volume reduction propagated toward the dorsal hippocampal region. Voxel-based analyses showed that atrophy originated from the EC in both the early and moderate stages and spread further into the hippocampus at the later stage. In addition, we performed voxel-based analyses on EC-Tau mice at a prepathological tau stage (6 to 12 months old; EC-Tau: $n = 9$, average age = 8.8 months; control: $n = 7$, average age = 9.2) to test whether tau transgene expression had any effect. No significant volume reduction was seen throughout the brain.

The in vivo MRI atlas was also used to identify which specific subregions of the MTL were affected. Figure 3 shows two representative

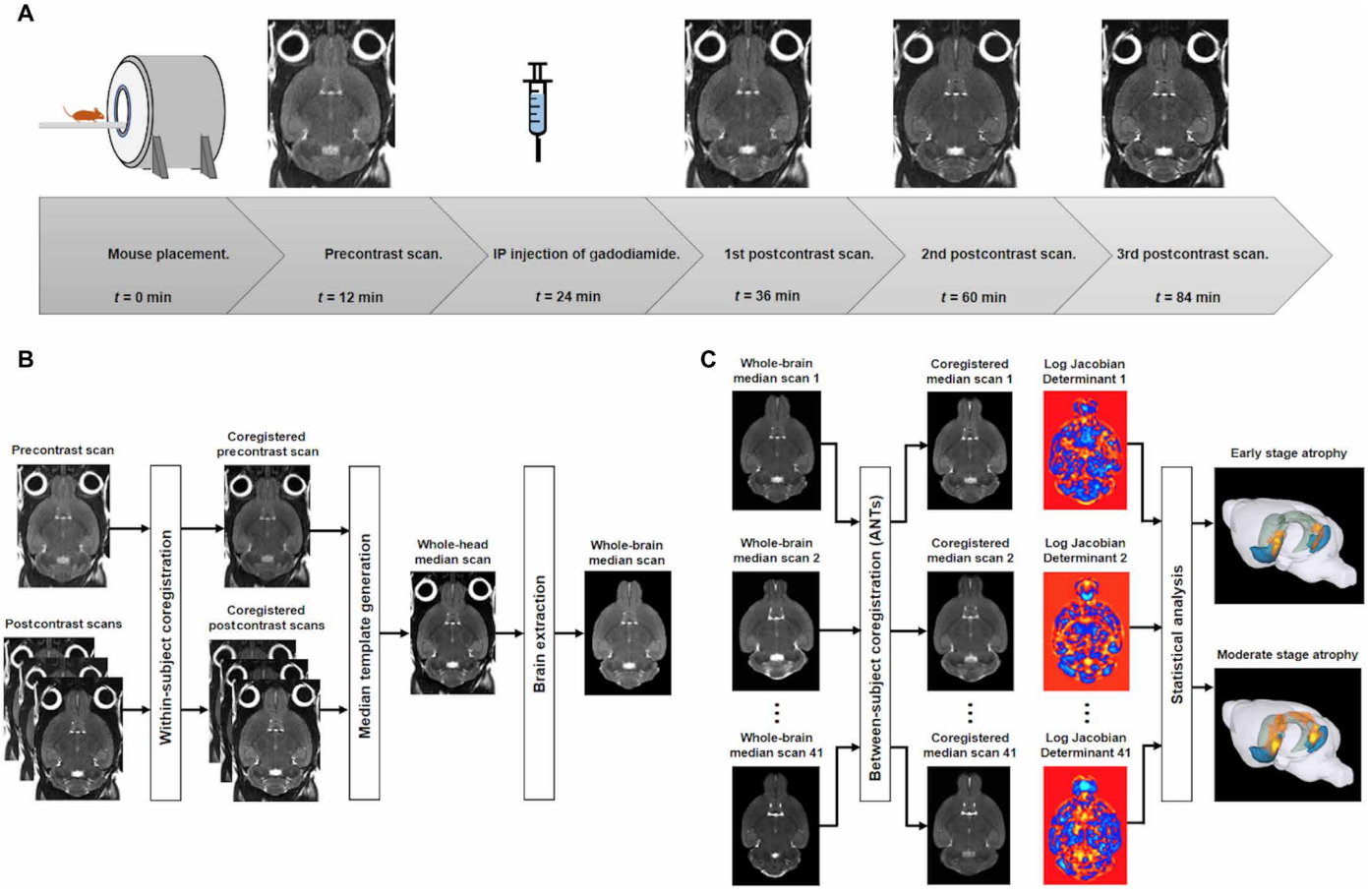

Fig. 1. Schematic showing the timeline for MRI image acquisition and image processing pipeline. (**A**) The mouse is placed into the MRI system, and a precontrast scan begins. Following intraperitoneal (IP) injection of gadodiamide, three consecutive postcontrast scans are acquired. (**B**) Generation of whole-brain median scan for one mouse. The pre- and postcontrast scans are iteratively aligned during within-subject coregistration, and the coregistered scans are used to generate a whole-head median scan. The median scan undergoes brain extraction and produces a whole-brain median scan. (**C**) Between-subject coregistration is performed using Advanced Normalization Tools (ANTs) to coregister all of the whole-brain median scans ($n = 41$). The median scans are coregistered into a group-wise template space and the logarithmic transform of the Jacobian determinant (log JD) of the warp for each mouse is generated. The log JD tensor map for each mouse is grouped according to their genotype (EC-Tau or control) and age (early stage: 20 to 24 months, or moderate stage: 30 to 36 months). Voxel-based statistical analyses are conducted using two-sample Student's *t* test to produce an atrophy map for the early stage and for the moderate stage.

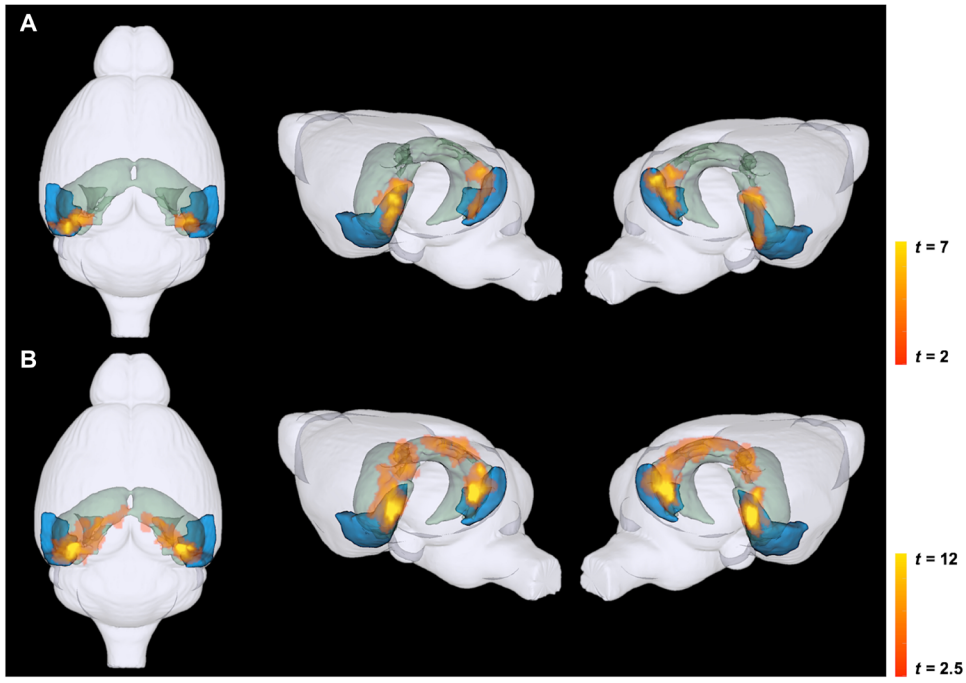

Fig. 2. 3D rendering of significant volume reduction in EC-Tau mice in the MTL at 20 to 24 months old (which represents an early stage in human AD tauopathy) and 30 to 36 months old (which represents a moderate stage). TBM-related atrophy in the EC and hippocampus at (**A**) early stage and (**B**) moderate stage. For each panel, the colored regions depict the EC (LEC and MEC) in blue and the hippocampus (DG, CA1, CA2, CA3, and dhc; subicular complex: Sub, PPS, and Post) in green. Each panel shows the top view (left), left hemisphere (middle), and right hemisphere (right) of the mouse brain. Voxel-based analyses were conducted using a general linear model in statistical parametric mapping (SPM), and individual genotypes at each stage were contrasted using two-sample Student's *t* test. Statistics are represented as heatmaps of *t* values corresponding to voxel-level $P < 0.005$ and cluster-level $P < 0.05$.

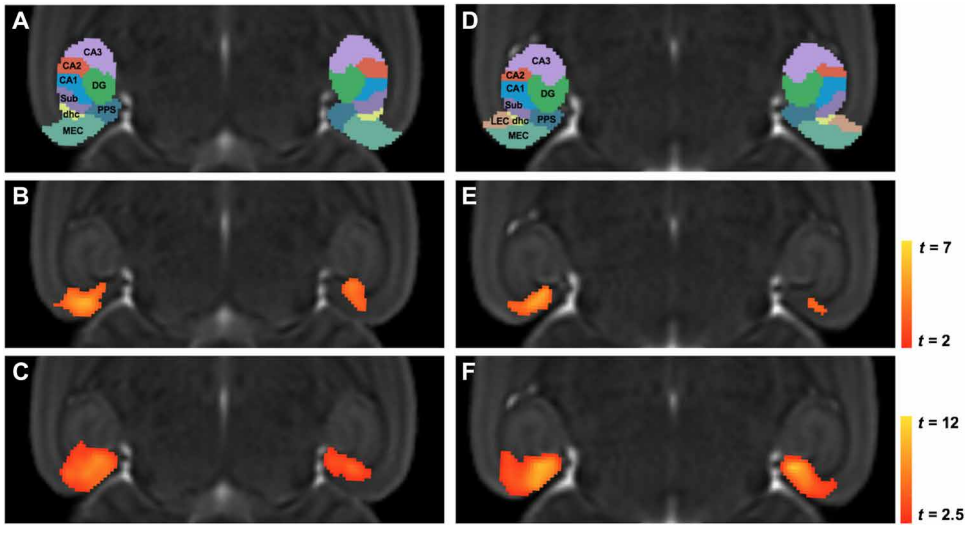

Fig. 3. Significant volume reduction in EC-Tau mice illustrated in 2D representative axial slices at the early stage (20 to 24 months) and at the moderate stage (30 to 36 months). TBM-related atrophy in a dorsal slice (left) and ventral slice (right). (**A** and **D**) In vivo MRI atlas label overlaid on a group-wise template defining subregions of the EC and hippocampus at (**B** and **E**) early stage and (**C** and **F**) moderate stage. Voxel-based analyses were conducted using a general linear model in SPM and individual genotypes at each stage were contrasted using two-sample Student's *t* test. Statistics are represented as heatmaps of *t* values corresponding to voxel-level $P < 0.005$ and cluster-level $P < 0.05$.

2D axial slices with the MTL atlas labels overlaid on the group-wise template in the top panels (Fig. 3, A and D) and the significant atrophy in the early and moderate stages in the middle (Fig. 3, B and E) and bottom panels (Fig. 3, C and F), respectively. At the early stage, the EC-Tau group showed significant volume reduction mainly in the MEC and PPS compared with their age-matched controls. Compared with the early stage, EC-Tau mice at the moderate stage had more significant atrophy in the regions that were initially affected, and atrophy had spread from these regions into the hippocampus and subicular complex.

Spread of TBM-related atrophy from EC into hippocampus

To quantify the spread of atrophy in the MTL between the early and moderate stages, we calculated the percentage of each subregion with significant volume reduction in the 3D volume. Table 1 shows the percentages for each subregion at both stages. Within the EC, the MEC showed the greatest effect, with 21.52% of the region showing significant volume reduction that increased to 28.72% at the moderate stage. The LEC was minimally affected at both the early and moderate stage. Although tau pathology was apparent in both the LEC and MEC in EC-Tau mice, previous ex vivo studies have shown that the tau transgene is expressed more abundantly in MEC neurons and that there was a relatively more intense tau immunolabeling (human tau antibody, CP27 antibody) in the MEC than in the LEC (*14*). The amount of tau pathology in the EC of left and right hemispheres was not significantly different. The degree of tau pathology in the MEC was associated with the significant volume reduction in this region and is explored in a later section. Of the hippocampal subregions, the CA1, DG, and Sub had the most notable increase in percentage of region with significant atrophy when comparing the two stages. The CA1 volume reduction increased from 0.21% at the early stage to 7.45% at the moderate stage. In the DG, 0.73% of the region was affected at the early stage that increased to 7.65% at the moderate stage. In addition, the Sub was greatly affected, from 13.45% (early stage) to 44.42% (moderate stage). The PPS, Post, and dhc, which contains projections of pre-Sub (PrS) from (and to) the EC (*19*), all showed significant volume reduction at the early stage and the percentage increased at the moderate stage. There was no significant volume reduction in the CA2 and negligible volume reduction in the CA3 at both the early and moderate stages.

Neuronal loss and volume reduction at the moderate stage

We investigated the relationship between neuronal loss and volume reduction in the EC, PPS, Sub, DG, and CA1 in EC-Tau mice compared with age-matched controls at the moderate stage. $NeuN^+$ neurons were counted in the EC of EC-Tau (Fig. 4A) and control mice (Fig. 4B) and in the PPS of EC-Tau (Fig. 4C) and control mice (Fig. 4D), as well as in the Sub, DG, and CA1 (fig. S1). Volume reduction analysis was performed on slices that matched the NeuN-immunolabeled sections. The number of $NeuN^+$ neurons significantly decreased in the EC [$t(8) = 4.129$, $P = 0.003$] and in the PPS [$t(18) = 6.476$, $P = 0.0002$] in the EC-Tau mice compared with controls, but not in the Sub [$t(8) = 0.421$, $P = 0.685$], DG [$t(8) = 0.784$, $P = 0.456$], or CA1 [$t(8) = 0.034$, $P = 0.974$] (Fig. 4E). There was also significant volume reduction in EC-Tau mice in the EC [$t(18) = 3.204$, $P = 0.005$] and in the PPS [$t(18) = 7.026$, $P = 1.479 \times 10^{-6}$], as well as in the Sub [$t(18) = 4.452$, $P = 0.0003$] and the molecular layer of the DG [MoDG; $t(18) = 2.628$, $P = 0.017$], but not in the CA1 [$t(18) = 0.958$, $P = 0.351$] (Fig. 4F). Thus, the significant volume reduction we observed in the Sub and MoDG precedes overt cell loss at the moderate stage.

3D imaging of iDISCO+ CP27 staining and TBM-related atrophy

To qualitatively visualize the association between tau pathology and significant volume reduction in EC-Tau mice, we coregistered iDISCO+ CP27 (human tau) immunolabeled data from a 25-month and a 34-month EC-Tau mouse with the early-stage and moderate-stage atrophy map, respectively (Fig. 5, B and C). Figure 5A shows a representative 3D model of the left hemisphere of the mouse brain with the EC in blue and the hippocampus in green. The CP27 antibody detects all human tau, regardless of conformation or phosphorylation status; however, accumulation in the somatodendritic compartment represents an early pathological stage. CP27 immunolabeling correlates well with the distribution of tau labeled with the MC1 antibody, which detects human tau in an abnormal pathological conformation (*20*). Our results showed human tau immunolabeling throughout the left hemisphere, but the tau labeling was more intense and extensive in the regions corresponding to significant volume reduction in the MTL (Fig. 5B). More specifically, human tau in the MEC and PPS corresponded with the significant atrophy in the same regions at the early stage. Compared with the early stage, less human tau was present throughout the MTL at the moderate stage due to the loss of neurons, but there was significant volume reduction in the EC and PPS and at this stage, in the hippocampus (Fig. 5C).

DISCUSSION

In AD, the first neurons to be affected with tauopathy are in layer II of the EC (*1*, *21*). This layer projects directly into the outer two-thirds of the MoDG (*22*), which together with projections to other subfields of the hippocampal formation forms the so-called perforant pathway (*23*). The perforant pathway also consists of projections from neurons in layer III of the EC to the Sub and CA1 (*23*). The Sub and, to a lesser extent, the CA1 form the main output from the hippocampus to the deeper layers of the EC, while the para-Sub (PaS) and PrS also have projections to and from the EC (*24*).

TBM is a noninvasive, automated imaging technique that has proven to be essential in identifying local structural differences in whole-brain analyses, providing high spatial and temporal resolution to determine the volumetric changes observed at multiple time points. In this study, we used TBM-MRI to map volume reduction in aging EC-Tau mice at two time points that represent two stages of tauopathy in human AD, early and moderate, and to investigate the association of tau pathology with the spread of volumetric reduction and neuronal loss between areas that are synaptically connected to the EC.

Table 1. Percentage of each subregion in the EC and hippocampus with significant volume reduction at the early and moderate stage.

	EC (%)		Hippocampus (%)							
	MEC	LEC	CA1	CA2	CA3	DG	Sub	PPS	Post	dhc
Early	21.52	0.22	0.21	0	0	0.73	13.45	41.18	17.49	33.51
Moderate	28.72	1.16	7.45	0	0.03	7.65	44.42	55.81	22.46	50.93

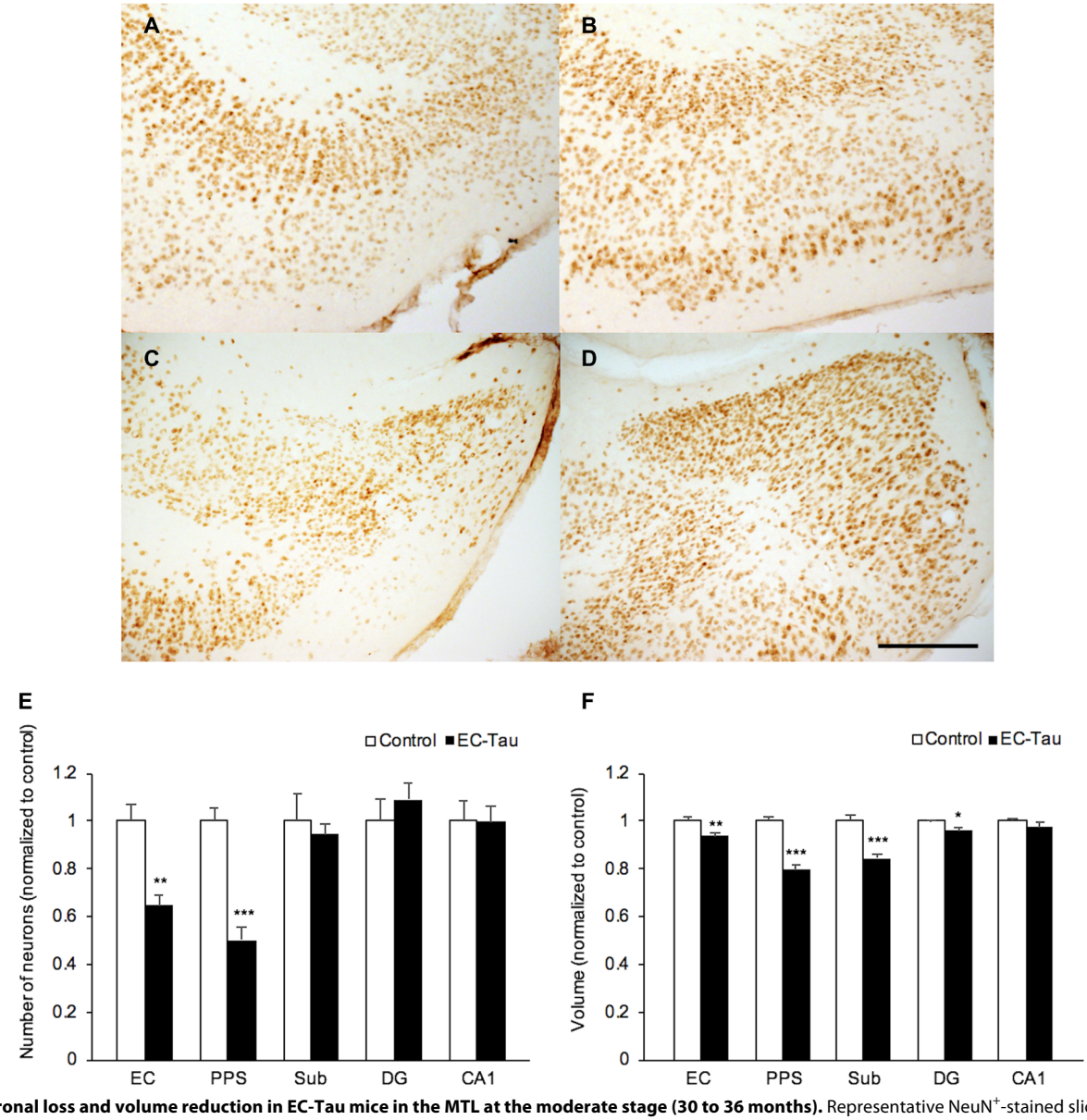

Fig. 4. Neuronal loss and volume reduction in EC-Tau mice in the MTL at the moderate stage (30 to 36 months). Representative NeuN$^+$-stained slice in the EC of (**A**) an EC-Tau mouse and (**B**) a control mouse and in the PPS of (**C**) an EC-Tau mouse and (**D**) a control mouse. Scale bar, 200 μm. (**E**) The mean number of neurons in each subregion was compared between control ($n = 5$) and EC-Tau ($n = 5$) mice at the moderate stage. (**F**) The mean volume of each subregion was calculated from the JD and compared between control ($n = 10$) and EC-Tau ($n = 10$) mice at the moderate stage. A two-sample two-tailed Student's *t* test was performed to analyze neuron counting and volume reduction. All data are expressed as means + SEM (*$P < 0.05$, **$P < 0.01$, and ***$P < 0.001$).

Our TBM-MRI data showed that most of the significant atrophy in the EC-Tau mouse line was located in the MTL region at both the early and moderate stage, with some affected regions adjacent to the MTL. This could be due to atrophy inside the MTL region causing these adjacent regions to show atrophy as well. By the moderate stage, widespread atrophy projected into the anterior-medial region of the hippocampus and subicular complex. With the whole-brain analysis, we were able to visualize atrophy throughout the entire brain and subsequently determine that the MTL showed the largest region of volume reduction at both the early and moderate stages. Using the coregistered in vivo atlas, we identified specific individual subregions in the EC and hippocampus with significant atrophy and demonstrated that atrophy originating in the MEC and PPS of the MTL spread into the CA1, DG, and Sub regions of the hippocampus and subicular complex.

Delineating the spatial and temporal spread of tau pathology along this pathway has been of emerging interest, but the implications for neurodegeneration have not been well explored. Ex vivo studies in the EC-Tau mouse line have shown that tau pathology in the EC spreads to functionally connected regions in the hippocampus as the mice age (*14*–*16*). Age-dependent structural changes such as axonal and synaptic degeneration occur in the EC by 21 months, but with no significant neuronal loss (*16*). By 24 months, both pre- and postsynaptic densities were significantly reduced in the middle third of the MoDG (*16*), suggesting that synapses are lost in this region as axons originating from neurons in the EC degenerate.

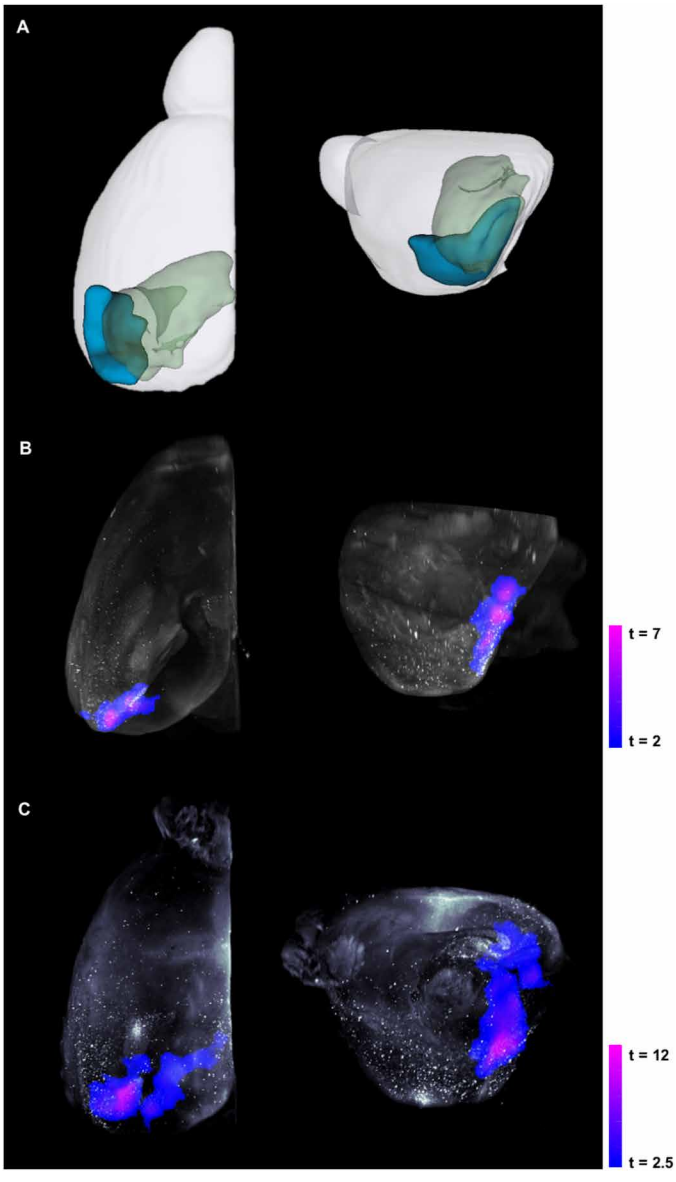

Fig. 5. 3D representation of iDISCO+ CP27 overlaid with significant volume reduction in the left hemisphere of the mouse brain. (**A**) Representative model of the left hemisphere of the mouse brain with the EC (LEC and MEC) in blue and the hippocampus (DG, CA1, CA2, CA3, and dhc; subicular complex: Sub, PPS, and Post) in green. iDISCO+ CP27 (white), which stains all human tau, was coregistered with TBM-related atrophy at (**B**) the early stage and (**C**) the moderate stage. Each panel shows the top view (left) and left hemisphere (right) of the mouse brain. Voxel-based analyses were conducted using a general linear model in SPM, and individual genotypes at each stage were contrasted using two-sample Student's *t* test. Statistics are represented as heatmaps of *t* values corresponding to voxel-level $P < 0.005$ and cluster-level $P < 0.05$.

In addition, significant neuronal loss was detected in the EC-II and PaS compared with the average neuron number in age-matched control brains (*15*, *16*, *25*). Axonal tau was markedly reduced and human tau accumulated in cell bodies in the EC and hippocampus (DG, CA1, CA2/3, Sub, and PrS) at 24 months (*15*). The relocation of tau from the axons to the somatodendritic compartment is one of the earliest events in the pathological cascade of early AD (*1*), and it is possible that axon degeneration is initiated in the EC. The progressive spread of tau pathology associated with the TBM-related atrophy that we see at the early stage (Figs. 2A and 3, B and E) suggests that atrophy is caused by axon degeneration and synaptic loss along the perforant pathway from the EC into the DG as well as neuronal loss in the EC and PaS. Whether atrophy is related to toxicity associated with non–cell autonomous spread of tau or due to cell-autonomous mechanisms of spread is not known.

EC-Tau mice at the moderate stage (approximately 34 months of age) had almost undetectable tau protein in axons, but the protein had accumulated in cell bodies throughout the hippocampal formation (*15*). At this age, the number of neurons was significantly reduced in the EC-II and PPS compared with age- and gender-matched control mice, as well as in the EC-III/IV, indicating progressive neuronal loss as pathology worsens and spreads in the brain (*15*). However, there was no significant neuronal loss detected in the CA1, DG, and Sub regions at 34 months in our ex vivo study (*15*). Our TBM-MRI study showed that the CA1, DG, and Sub regions displayed the greatest increase in percentage of significant volume reduction at the moderate stage (Table 1). We selected slices that matched the $NeuN^+$-stained sections to further explore the relationship between neuronal loss (Fig. 4E) and volume reduction (Fig. 4F). There was significant neuronal loss and volume reduction in both the EC and PPS. In addition, the Sub and MoDG showed significant volume reduction, but no significant neuronal loss. Our finding indicates that the volume reduction in the Sub and MoDG precedes overt cell loss at the moderate stage.

Neuron loss is associated with the presence of NFTs that were shown to be mature tangles by thioflavin S staining (*14*–*16*). Compared with mice at 24 months of age, larger aggregates composed of thioflavin S–positive tau were only observed in the EC and PPS at 34 months (*25*), which correlated with the neuron loss observed in these regions (*15*). This suggests that the volume reduction we observed at the moderate stage in the MoDG and Sub is due to the dysfunction and degeneration of regions directly connected to the EC rather than the presence of NFTs and neuron loss. The atrophy is possibly due to the axon and synapse degeneration initiated in the EC, primarily along the perforant pathway into the MoDGs (*16*). Also, the death of neurons in the EC and PPS could induce degeneration in secondary regions that are directly connected because of the lack of input from the neurons in the EC. This is a result of the connectivity within the trisynaptic circuit, which is composed of three excitatory synapses (EC-II ➔ DG ➔ CA3 ➔ CA1), associational loops, and partly complex interneuronal circuits (*26*). The CA1 and Sub form projections to the deeper layers of the EC, whereas the PaS and PrS have projections to and from the EC (*24*). It is likely that neuronal loss and degeneration in these regions as a result of pathological tau accumulation affect this interconnected network. In summary, using TBM-MRI, we could not only pinpoint specific regions in the brain with atrophy, but we were also able to visualize these changes throughout circuits, in 3D. Our findings show that not only can we map the structural changes previously observed in ex vivo studies, but we can also demonstrate that progressive neurodegeneration precedes overt cell loss in the MoDG and Sub.

Using data generated in our previous study (*15*), we coregistered our 3D TBM-MRI atrophy results with 3D imaging using iDISCO+ immunolabeling of human tau in EC-Tau mice at both the early and moderate stages (Fig. 5). Coregistration of human tau pathology

and the TBM-related atrophy results mapped the spatial accumulation of human tau to examine the association with structural changes in corresponding regions. Immunolabeled, somatic human tau was most prevalent in the MEC and PPS region that corresponded to the same regions with the highest atrophy in our TBM-MRI results at the early stage. At the moderate stage, less human tau was apparent in the MTL region, while there was still an increase and spread of atrophy from the EC into the hippocampus. This finding indicates that degeneration in the hippocampus is subsequent to the degeneration originating in the EC. As discussed earlier, ex vivo studies detected neuronal loss in the EC-II and PaS at 24 months (*15*) and in the EC-II, EC-III/IV, and PPS at 34 months, but not in the hippocampal subregions such as the CA1, DG, and Sub (*15*). This, together with the coregistered 3D iDISCO+ imaging and TBM-MRI atrophy results, further supports the interpretation that the spread of tau pathology is associated with synaptic/axonal degeneration and neuronal loss at the early stage, but at the moderate stage, the atrophy we observe in the MoDG and Sub is not due to neuronal loss. TBM-MRI allowed us to visualize this volume reduction in aged EC-Tau mice, originating from the EC and propagating into the hippocampus. At both stages, the left hemisphere was more affected compared with the right hemisphere, although there was no overt difference in tau pathology between hemispheres. Several studies have looked at cerebral volume asymmetry in both rodents and humans (*27*–*33*). However, it is currently unknown why structural and functional laterality differences occur in rodents and humans.

Recent studies in humans examined the association between tau accumulation with PET imaging tracers and cortical atrophy using structural MRI. A significant negative relationship between tracer uptake and concurrent cortical thickness was observed in the MTL (*9*–*12*), as well as in regions outside of the MTL and in neocortical areas such as the temporoparietal, posterior cingulate/precuneus, and occipital cortices (*5*–*7*, *9*–*13*). In a recent longitudinal study, the global intensity of tau-PET signal, but not β-amyloid (Aβ)–PET signal, predicted the rate of subsequent atrophy (*13*). In addition, the specific distribution of tau-PET signal was a strong indicator of the topography of future atrophy at the single patient level (*13*). This supports our results showing that the spread of atrophy is associated with tau pathology in the EC-Tau line and demonstrates the utility of transgenic tau mouse models to study the molecular drivers of these effects.

There have been some inconsistencies in the relationship between tau accumulation with PET imaging and hippocampal atrophy with MRI. Some studies have shown that while there was significant atrophy in the hippocampus, there was no significant difference in hippocampal PET tracer retention between the AD patients and controls (*34*, *35*). The discrepancy between tau deposits and cortical atrophy may be due to several factors. First, Aβ status—some studies show that atrophy is preferentially associated with tau rather than Aβ pathology (*5*–*7*); second, lack of extensive validation of existing tau-specific PET tracers—the type of tau deposits (conformation, maturation stage, tau isoform), their specific binding site(s), and "off-target" binding may affect the sensitivity and specificity of tracers (*36*–*38*); and third, the absence of longitudinal data in some studies—further longitudinal data are necessary to clarify the spatiotemporal relationships between tau deposition and atrophy (*5*, *10*, *11*, *34*). Our study overcomes these limitations by using a transgenic tau mouse model to examine the relationship between tau pathology (as opposed to amyloid plus tau pathology) and atrophy, and its association with neurodegeneration, at two stages of disease. It is not possible to separate out these factors in human studies.

In conclusion, we demonstrate that TBM-MRI is an effective, noninvasive imaging technique that can determine which individual regions of the brain are affected at different stages during disease progression. Although TBM-MRI does not allow us to identify the underlying causes of atrophy, this method is sensitive enough to detect atrophy in brain subfields and can guide ex vivo experiments designed to analyze neuronal vulnerability at a molecular level. While our study focused primarily on volumetric changes in the MTL region at two time points, additional research can be conducted to longitudinally track the reduction (or expansion) of volume in other regions with whole-brain analyses. Thus, TBM-MRI can enhance our understanding of the pathological basis and progression of neurodegeneration in AD and other neurodegenerative disorders.

MATERIALS AND METHODS

Study design

In our study, we conducted a blinded, controlled laboratory experiment with transgenic EC-Tau mice aged 20 to 24 months old (early stage) and 30 to 36 months old (moderate stage) compared with their age-matched littermates. The animal subjects were randomly assigned to experimental groups based on their age (early or moderate stage) and genotype (EC-Tau or control). The animal caretakers provided the mice based on mouse ID number, and the animal data were scanned in the MRI and processed randomly. The investigators who assessed, measured, and quantified the results were blinded to the genotype of each group. A power analysis was performed to calculate the necessary sample size for each group. Estimates for group sizes per study were based on effect sizes observed in past experiments investigating volume changes in the brain using the logarithmic transform of the Jacobian determinant (JD). Effect sizes have been approximately 0.08, and SDs have been approximately 0.06. These values are used in the following formula to obtain a sample size estimate for an unpaired t test: $n = 1 + 16 \times ([\text{SD}] / [\text{effect size}])^2$. The sample size we arrive at is $n = 10$ animals for each experimental group and $n = 10$ for each control group.

The criteria for inclusion and exclusion of data were established prospectively based on SNR (signal-to-noise ratio) of each mouse scan. Typical SNR values range between 15 and 25 (*39*). MRI scans with an SNR in the typical range were included in the data, and scans with an SNR outside of this range were excluded from the study. An outlier is a value that is more than three scaled median absolute deviations away from the median and was defined before the beginning of this study. No outliers were detected during the study. This study was conducted on a per subject basis and no replicates were applied.

Previous ex vivo studies show structural changes such as axonal and synaptic degeneration in the EC and DG of the hippocampus in EC-Tau mice compared with control mice at the early stage (*15*, *16*), while significant neuronal loss was only detected in the EC-II and PaS (*16*). At the moderate stage, tau protein had spread and accumulated throughout the hippocampal formation, but neuronal loss was only seen in the EC and PPS (*15*). Our study aims to delineate the association of tau pathology with the spread of TBM-MRI volume reduction and neuronal loss observed with $NeuN^+$ staining. Furthermore, we qualitatively visualized the association of tau pathology with iDISCO+ CP27 immunolabeled data and our TBM-MRI volume reduction results.

Transgenic mice

An inducible mouse line in which the expression of human full-length tauP301L (EC-Tau) (*14*, *15*) was predominant in the EC was created by crossing the neuropsin-tTA "activator" line [genotype, Tg(Klk8-tTA)SMmay/MullMmmh; strain background, congenic on C57BL/6 background] (*40*) with a tetracycline-inducible "responder" line [genotype, Tg(tetO-MAPT*P301L)#Kha/JlwsJ; strain background, FVB/N background] (*41*) to create the bigenic EC-Tau line and control nontransgenic littermates [Tg(Klk8-tTA)SMmay/MullMmmh Tg(tetO-MAPT*P301L)#Kha/JlwsJ; strain background, FVB/N:C57BL/6] (*14*). Experimental mice were all F1 progeny. The mice were separated into two age groups representing early (20 to 24 months old; EC-Tau: $n = 11$, average age = 20.71 months; control: $n = 10$, average age = 20.70 months) and moderate (30 to 36 months old; EC-Tau: $n = 10$, average age = 33.38 months; control: $n = 10$, average age = 32.26 months) stages of tauopathy (approximately equivalent to human AD Braak stages I/II and Braak stages III/IV, respectively). Care of transgenic mice was in accordance with protocol approved by the Institutional Animal Care and Use Committee at the Columbia University.

Image acquisition

MRI images were acquired with a 9.4-T vertical Bruker magnet and a 30-mm inner diameter birdcage radio frequency coil before and after intraperitoneal injections of contrast agent gadodiamide (10 mmol kg^{-1}) (*33*, *39*). Three postcontrast scans were acquired after intraperitoneal injection. Mice were anesthetized with isoflurane mixed with oxygen delivered through a nose cone (2% for induction, 1 to 1.5% for maintenance during scan). T2-weighted images were obtained using a fast spin echo sequence with repetition time (TR) = 3500 ms, echo time (TE) = 15 ms, effective TE = 43.84 ms, in-plane resolution = 86 μm, and slice thickness = 500 μm. Figure 1A shows the timeline for MRI image acquisition.

Image analysis

Using a robust, symmetric method (*42*), an unbiased, within-subject coregistration was performed by iteratively aligning the pre- and postcontrast images for each mouse (*43*). A gadolinium-enhanced MRI image for each animal was calculated as the median of all four processed T2-weighted images to ensure high structural contrast (*44*). The whole-head median scans were skull stripped using a pulse-coupled neural network algorithm optimized for rodent brains that operates in 3D (*45*) to produce whole-brain volumes (Fig. 1B). The whole-brain median scans were then up-sampled to an isotropic resolution of $86 \times 86 \times 86\ \mu m^3$ using mri_convert (FreeSurfer) with cubic interpolation.

Between-subject coregistration was performed using Advanced Normalization Tools (ANTs) (*46*, *47*) to transform individual median scans into a group-wise template space. First, a linear transformation with 12 degrees of freedom using a cross-correlation (CC) intensity-based similarity metric was optimized to globally align the median scans to a randomly selected image in their dataset. Using the linearly aligned images, the optimal Greedy "Symmetric Normalization" (SyN) diffeomorphic transformation was then determined to produce the necessary deformations to warp each median scan into the group-wise template space. The coregistration algorithm was instantiated by the ANTs script buildparalleltemplate.sh. Last, the linear transformation and nonlinear warps were applied with the ANTs program WarpImageMultiTransform to transform the median scan for each mouse into the group-wise template space. This state-of-the-art SyN method for maximizing CC is a reliable method for normalizing and making anatomical measurements in volumetric MRI in neurodegenerative brain (*47*).

TBM is an image analysis technique that identifies regional structural differences from the gradients of the nonlinear deformation fields or warps (*17*). The logarithmic transformation of a Jacobian field is a common metric used to evaluate these structural differences at a voxel level and has become a standard in TBM (*48*–*50*). Using the ANTs program ANTSJacobian, the JD of the warp and the logarithmic transform of the JD (log JD) of the warp for each mouse was generated to determine the structural changes between the EC-Tau mice and controls for each age group (Fig. 1C).

Atlas-based segmentation

An in vivo MRI atlas of the mouse brain was constructed to determine which specific subregions of the brain are affected. To do this, an ex vivo MRI mouse brain atlas (Australian Mouse Brain Mapping Consortium) with hippocampus (*19*) and cortex (*51*) labels was used. Subregional segmentation was fitted to the symmetric model (*52*) to avoid left/right average differences. First, the symmetric model mouse brain, hippocampus labels, and cortex labels were down-sampled to an isotropic resolution of $86 \times 86 \times 86\ \mu m^3$ using mri_convert (FreeSurfer). Similarly, the group-wise template was up-sampled to a matching isotropic resolution. The hippocampus and cortex regions were manually masked on both the symmetric model mouse brain and group-wise template to yield volumes containing regions of interest. Using the ANTs script mentioned earlier, the masked symmetric model brain was registered to the masked group-wise template using a linear transformation with a CC similarity metric, followed by a Greedy SyN transformation to determine the necessary deformations to warp the symmetric model brain into the group-wise template space. With the ANTs program, the linear transformation and nonlinear warps were applied to the hippocampus and cortex labels and overlaid on the group-wise template image in 3DSlicer (www.slicer.org).

Voxel-based statistical analysis

Voxel-based analyses were conducted using a general linear model in statistical parametric mapping (Wellcome Trust Centre for Neuroimaging). The log JD tensor maps of individual genotypes at each stage (early: $n = 11$ EC-Tau, $n = 10$ control; moderate: $n = 10$ EC-Tau, $n = 10$ control) were contrasted using two-sample Student's t test. Results were corrected for multiple comparisons using Monte Carlo simulation implemented in AFNI-AlphaSim (*53*) with 5000 iterations to achieve a voxel-wise $P < 0.005$ and cluster-wise $P < 0.05$. The thresholded t maps from individual group comparisons were then overlaid on the group-wise template image in 3DSlicer (www.slicer.org) with the registered hippocampus and cortex labels (Fig. 1C).

Percentage of subregions with significant volume reduction

The percentage of each subregion with significant volume reduction in the EC and hippocampus was calculated to quantify the spread between the early and moderate stage. First, we used the thresholded t map for each age group to create a binary image labeled with value 1 for voxels with significant volume reduction and value 0 for all other voxels that were not affected. Using the in vivo MRI atlas and a custom MATLAB script, we calculated the number of voxels in

each subregion of the MTL labeled with value 1 and divided by the total number of voxels in each subregion to determine the percentage of voxels affected in both the early and moderate stage.

Neuronal counts and volume reduction analysis at moderate stage

Data from neuronal counts were modified from Fu *et al.* (*15*) and incorporated in our study. Briefly, mouse brains (n = 5 controls, n = 5 EC-Tau mice at ~34 months old) were harvested and drop fixed in 4% paraformaldehyde (PFA) at 4°C overnight, followed by incubation in 30% sucrose (Sigma-Aldrich, Saint Louis, MO, USA). Optimal cutting temperature (OCT)–embedded brains were sectioned (35 μm) throughout on a horizontal (axial) plane with a cryostat (Leica CM3050S, Leica Biosystems, Buffalo Grove, IL, USA) and collected in individual wells. Every ninth free-floating section was selected and stained with mouse anti-NeuN antibody (EMD Millipore, Billerica, MA, USA; 1:1000), which is a neuronal marker. A semiquantitative count of $NeuN^+$ neurons in the EC, PPS, Sub, CA1, and DG was performed in the above-selected sections. For each mouse, a total of 10 NeuN-stained horizontal sections starting from bregma −2.04 mm, spaced at 300 μm, were included for automated cell counting (http://imagej.net/Particle_Analysis) using the ImageJ software (version 1.48, U.S. National Institutes of Health, Bethesda, Maryland, USA).

Similarly, the coregistered JDs of the warp for each mouse in the moderate stage (n = 10 control, n = 10 EC-Tau, 30 to 36 months old) were used to observe the relationship between atrophy and $NeuN^+$ neurons in the same regions, as mentioned above. Slices from the JD of each mouse were selected to match the NeuN-stained sections. Using a custom MATLAB code and the MRI atlas, the sum of the JD for each subregion was calculated for each mouse in the moderate stage.

Statistical analysis

The data are expressed as the means ± SEM. A two-sample two-tailed Student's t test was used to analyze the neuronal counting (n = 5 controls, n = 5 EC-Tau mice) and the volume reduction in mice (n = 10 controls, n = 10 EC-Tau) at the moderate stage. A value of $P < 0.05$ was considered statistically significant.

iDISCO+ CP27 staining and TBM-related atrophy coregistration

As previously described (*15*), the 3D iDISCO+ immunolabeled datasets of Alexa Fluor 647–labeled CP27 antibody (conformation and phosphorylation status independent) in a 25-month-old EC-Tau mouse and a 34-month-old EC-Tau mouse were used to represent the early stage and moderate stage, respectively. Using the Imaris software, the 3D iDISCO+ datasets were exported as a stack of 2D slices. The datasets were down-sampled to an isotropic resolution of 86 × 86 × 86 μm^3 using mri_convert (FreeSurfer) to match the resolution of the MRI group-wise template. Coregistration between the iDISCO+ dataset and their respective age-matched group-wise template was performed using ANTs as mentioned previously. A linear transformation with 12 degrees of freedom using a CC similarity metric was implemented to align the two datasets. Using the linearly aligned datasets, the optimal Greedy SyN diffeomorphic transformation was then determined to produce the necessary deformations to warp the group-wise template into the iDISCO+ data template space. Last, the linear transformation and nonlinear warps were applied to the voxel-based thresholded t maps for both age groups. This transformation coregistered the voxel-based atrophy results with their age-matched iDISCO+ pathology data. The coregistered atrophy data were overlaid on the iDISCO+ pathology data and visualized in 3D using the Imaris software.

SUPPLEMENTARY MATERIALS

Supplementary material for this article is available at http://advances.sciencemag.org/cgi/content/full/6/42/eabc8098/DC1

View/request a protocol for this paper from *Bio-protocol*.

REFERENCES AND NOTES

1. H. Braak, E. Braak, Neuropathological stageing of Alzheimer-related changes. *Acta Neuropathol.* **82**, 239–259 (1991).
2. P. Barbier, O. Zejneli, M. Martinho, A. Lasorsa, V. Belle, C. Smet-Nocca, P. O. Tsvetkov, F. Devred, I. Landrieu, Role of Tau as a microtubule-associated protein: Structural and functional aspects. *Front. Aging Neurosci.* **11**, 204 (2019).
3. E. Swanson, L. Breckenridge, L. McMahon, S. Som, I. McConnell, G. S. Bloom, Extracellular Tau oligomers induce invasion of endogenous Tau into the somatodendritic compartment and axonal transport dysfunction. *J. Alzheimers Dis.* **58**, 803–820 (2017).
4. A. Kneynsberg, B. Combs, K. Christensen, G. Morfini, N. M. Kanaan, Axonal degeneration in tauopathies: Disease relevance and underlying mechanisms. *Front. Neurosci.* **11**, 572–572 (2017).
5. E. Mak, R. A. I. Bethlehem, R. Romero-Garcia, S. Cervenka, T. Rittman, S. Gabel, A. Surendranathan, R. W. Bevan-Jones, L. Passamonti, P. Vázquez Rodríguez, L. Su, R. Arnold, G. B. Williams, Y. T. Hong, T. D. Fryer, F. I. Aigbirhio, J. B. Rowe, J. T. O'Brien, In vivo coupling of tau pathology and cortical thinning in Alzheimer's disease. *Alzheimers Dement.* **10**, 678–687 (2018).
6. R. Ossenkoppele, R. Smith, T. Ohlsson, O. Strandberg, N. Mattsson, P. S. Insel, S. Palmqvist, O. Hansson, Associations between tau, Aβ, and cortical thickness with cognition in Alzheimer disease. *Neurology* **92**, e601–e612 (2019).
7. B. A. Gordon, A. McCullough, S. Mishra, T. M. Blazey, Y. Su, J. Christensen, A. Dincer, K. Jackson, R. C. Hornbeck, J. C. Morris, B. M. Ances, T. L. S. Benzinger, Cross-sectional and longitudinal atrophy is preferentially associated with tau rather than amyloid β positron emission tomography pathology. *Alzheimers Dement.* **10**, 245–252 (2018).
8. T. M. Harrison, R. La Joie, A. Maass, S. L. Baker, K. Swinnerton, L. Fenton, T. J. Mellinger, L. Edwards, J. Pham, B. L. Miller, G. D. Rabinovici, W. J. Jagust, Longitudinal tau accumulation and atrophy in aging and alzheimer disease. *Ann. Neurol.* **85**, 229–240 (2019).
9. M. R. LaPoint, J. P. Chhatwal, J. Sepulcre, K. A. Johnson, R. A. Sperling, A. P. Schultz, The association between tau PET and retrospective cortical thinning in clinically normal elderly. *Neuroimage* **157**, 612–622 (2017).
10. C. Xia, S. J. Makaretz, C. Caso, S. McGinnis, S. N. Gomperts, J. Sepulcre, T. Gomez-Isla, B. T. Hyman, A. Schultz, N. Vasdev, K. A. Johnson, B. C. Dickerson, Association of in vivo [^{18}F]AV-1451 Tau PET imaging results with cortical atrophy and symptoms in typical and atypical Alzheimer disease. *JAMA Neurol.* **74**, 427–436 (2017).
11. S. R. Das, L. Xie, L. E. M. Wisse, R. Ittyerah, N. J. Tustison, B. C. Dickerson, P. A. Yushkevich, D. A. Wolk, Longitudinal and cross-sectional structural magnetic resonance imaging correlates of AV-1451 uptake. *Neurobiol. Aging* **66**, 49–58 (2018).
12. L. Wang, T. L. Benzinger, Y. Su, J. Christensen, K. Friedrichsen, P. Aldea, J. McConathy, N. J. Cairns, A. M. Fagan, J. C. Morris, B. M. Ances, Evaluation of Tau imaging in staging Alzheimer disease and revealing interactions between β-amyloid and tauopathy. *JAMA Neurol.* **73**, 1070–1077 (2016).
13. R. La Joie, A. V. Visani, S. L. Baker, J. A. Brown, V. Bourakova, J. Cha, K. Chaudhary, L. Edwards, L. Iaccarino, M. Janabi, O. H. Lesman-Segev, Z. A. Miller, D. C. Perry, J. P. O'Neil, J. Pham, J. C. Rojas, H. J. Rosen, W. W. Seeley, R. M. Tsai, B. L. Miller, W. J. Jagust, G. D. Rabinovici, Prospective longitudinal atrophy in Alzheimer's disease correlates with the intensity and topography of baseline tau-PET. *Sci. Transl. Med.* **12**, eaau5732 (2020).
14. L. Liu, V. Drouet, J. W. Wu, M. P. Witter, S. A. Small, C. Clelland, K. Duff, Trans-synaptic spread of Tau pathology in vivo. *PLOS ONE* **7**, e31302 (2012).
15. H. Fu, S. A. Hussaini, S. Wegmann, C. Profaci, J. D. Daniels, M. Herman, S. Emrani, H. Y. Figueroa, B. T. Hyman, P. Davies, K. E. Duff, 3D visualization of the temporal and spatial spread of Tau pathology reveals extensive sites of Tau accumulation associated with neuronal loss and recognition memory deficit in aged Tau transgenic mice. *PLOS ONE* **11**, e0159463 (2016).
16. A. de Calignon, M. Polydoro, M. Suárez-Calvet, C. William, D. H. Adamowicz, K. J. Kopeikina, R. Pitstick, N. Sahara, K. H. Ashe, G. A. Carlson, T. L. Spires-Jones, B. T. Hyman, Propagation of tau pathology in a model of early Alzheimer's disease. *Neuron* **73**, 685–697 (2012).
17. J. T. Ashburner, K. J. Friston, *Human Brain Function*, R. S. J. Frackowiak, K. J. Friston, C. D. Frith, R. J. Dolan, C. J. Price, S. Zeki, J. T. Ashburner, W. D. Penny, Eds. (Academic Press, Burlington, ed. 2, 2004), pp. 707–722.

18. J. Guo, Adapting and Optimizing CBV-MRI and MEGAPRESS-MRS to Measure Slow Functional Changes in Normal and Abnormal Brains, Dissertation, 2018, Columbia University.
19. K. Richards, C. Watson, R. F. Buckley, N. D. Kurniawan, Z. Yang, M. D. Keller, R. Beare, P. F. Bartlett, G. F. Egan, G. J. Galloway, G. Paxinos, S. Petrou, D. C. Reutens, Segmentation of the mouse hippocampal formation in magnetic resonance images. *Neuroimage* **58**, 732–740 (2011).
20. G. A. Jicha, R. Bowser, I. G. Kazam, P. Davies, Alz-50 and MC-1, a new monoclonal antibody raised to paired helical filaments, recognize conformational epitopes on recombinant tau. *J. Neurosci. Res.* **48**, 128–132 (1997).
21. T. Gómez-Isla, J. L. Price, D. W. McKeel Jr., J. C. Morris, J. H. Growdon, B. T. Hyman, Profound loss of layer II entorhinal cortex neurons occurs in very mild Alzheimer's disease. *J. Neurosci.* **16**, 4491–4500 (1996).
22. B. T. Hyman, L. J. Kromer, G. W. van Hoesen, Reinnervation of the hippocampal perforant pathway zone in Alzheimer's disease. *Ann. Neurol.* **21**, 259–267 (1987).
23. M. P. Witter, *Progress in Brain Research*, H. E. Scharfman, Ed. (Elsevier, 2007), vol. 163, pp. 43–61.
24. N. M. van Strien, N. L. M. Cappaert, M. P. Witter, The anatomy of memory: An interactive overview of the parahippocampal–hippocampal network. *Nat. Rev. Neurosci.* **10**, 272–282 (2009).
25. H. Fu, G. A. Rodriguez, M. Herman, S. Emrani, E. Nahmani, G. Barrett, H. Y. Figueroa, E. Goldberg, S. A. Hussaini, K. E. Duff, Tau pathology induces excitatory neuron loss, grid cell dysfunction, and spatial memory deficits reminiscent of early Alzheimer's disease. *Neuron* **93**, 533–541.e5 (2017).
26. J. Stepan, J. Dine, M. Eder, Functional optical probing of the hippocampal trisynaptic circuit in vitro: Network dynamics, filter properties, and polysynaptic induction of CA1 LTP. *Front. Neurosci.* **9**, 160–160 (2015).
27. S. Spring, J. P. Lerch, M. K. Wetzel, A. C. Evans, R. M. Henkelman, Cerebral asymmetries in 12-week-old C57Bl/6J mice measured by magnetic resonance imaging. *Neuroimage* **50**, 409–415 (2010).
28. J. P. Lister, J. Tonkiss, G. J. Blatt, T. L. Kemper, W. A. DeBassio, J. R. Galler, D. L. Rosene, Asymmetry of neuron numbers in the hippocampal formation of prenatally malnourished and normally nourished rats: A stereological investigation. *Hippocampus* **16**, 946–958 (2006).
29. C. Gaser, S. Schmidt, M. Metzler, K.-H. Herrmann, I. Krumbein, J. R. Reichenbach, O. W. Witte, Deformation-based brain morphometry in rats. *Neuroimage* **63**, 47–53 (2012).
30. O. Pedraza, D. Bowers, R. Gilmore, Asymmetry of the hippocampus and amygdala in MRI volumetric measurements of normal adults. *J. Int. Neuropsychol. Soc.* **10**, 664–678 (2004).
31. M. P. Pegues, L. J. Rogers, D. Amend, S. Vinogradov, R. F. Deicken, Anterior hippocampal volume reduction in male patients with schizophrenia. *Schizophr. Res.* **60**, 105–115 (2003).
32. F. Shi, B. Liu, Y. Zhou, C. Yu, T. Jiang, Hippocampal volume and asymmetry in mild cognitive impairment and Alzheimer's disease: Meta-analyses of MRI studies. *Hippocampus* **19**, 1055–1064 (2009).
33. U. A. Khan, L. Liu, F. A. Provenzano, D. E. Berman, C. P. Profaci, R. Sloan, R. Mayeux, K. E. Duff, S. A. Small, Molecular drivers and cortical spread of lateral entorhinal cortex dysfunction in preclinical Alzheimer's disease. *Nat. Neurosci.* **17**, 304–311 (2013).
34. Y. Shigemoto, D. Sone, E. Imabayashi, N. Maikusa, N. Okamura, S. Furumoto, Y. Kudo, M. Ogawa, H. Takano, Y. Yokoi, M. Sakata, T. Tsukamoto, K. Kato, N. Sato, H. Matsuda, Dissociation of Tau deposits and brain atrophy in early Alzheimer's disease: A combined positron emission tomography/magnetic resonance imaging study. *Front. Aging Neurosci.* **10**, 223 (2018).
35. D. Sone, E. Imabayashi, N. Maikusa, N. Okamura, S. Furumoto, Y. Kudo, M. Ogawa, H. Takano, Y. Yokoi, M. Sakata, T. Tsukamoto, K. Kato, H. Matsuda, Regional tau deposition and subregion atrophy of medial temporal structures in early Alzheimer's disease: A combined positron emission tomography/magnetic resonance imaging study. *Alzheimers Demen.* **9**, 35–40 (2017).
36. N. Okamura, R. Harada, A. Ishiki, A. Kikuchi, T. Nakamura, Y. Kudo, The development and validation of tau PET tracers: Current status and future directions. *Clin. Transl. Imaging* **6**, 305–316 (2018).
37. A. Leuzy, K. Chiotis, L. Lemoine, P.-G. Gillberg, O. Almkvist, E. Rodriguez-Vieitez, A. Nordberg, Tau PET imaging in neurodegenerative tauopathies—Still a challenge. *Mol. Psychiatry* **24**, 1112–1134 (2019).
38. L. Saint-Aubert, L. Lemoine, K. Chiotis, A. Leuzy, E. Rodriguez-Vieitez, A. Nordberg, Tau PET imaging: Present and future directions. *Mol. Neurodegener.* **12**, 19 (2017).
39. H. Moreno, F. Hua, T. Brown, S. Small, Longitudinal mapping of mouse cerebral blood volume with MRI. *NMR Biomed.* **19**, 535–543 (2006).
40. M. Yasuda, M. R. Mayford, CaMKII activation in the entorhinal cortex disrupts previously encoded spatial memory. *Neuron* **50**, 309–318 (2006).
41. K. Santacruz, J. Lewis, T. Spires, J. Paulson, L. Kotilinek, M. Ingelsson, A. Guimaraes, M. DeTure, M. Ramsden, E. McGowan, C. Forster, M. Yue, J. Orne, C. Janus, A. Mariash, M. Kuskowski, B. Hyman, M. Hutton, K. H. Ashe, Tau suppression in a neurodegenerative mouse model improves memory function. *Science* **309**, 476–481 (2005).
42. M. Reuter, H. D. Rosas, B. Fischl, Highly accurate inverse consistent registration: A robust approach. *Neuroimage* **53**, 1181–1196 (2010).
43. M. Reuter, N. J. Schmansky, H. D. Rosas, B. Fischl, Within-subject template estimation for unbiased longitudinal image analysis. *Neuroimage* **61**, 1402–1418 (2012).
44. X. Feng, J. Guo, H. Sigmon, R. Sloan, A. M. Brickman, F. A. Provenzano, S. Small, Brain regions vulnerable and resistant to aging without Alzheimer's disease. *PLOS ONE* **15**, e0234255 (2020).
45. N. Chou, J. Wu, J. B. Bingren, A. Qiu, K.-H. Chuang, Robust automatic rodent brain extraction using 3-D pulse-coupled neural networks (PCNN). *IEEE Trans. Image Process.* **20**, 2554–2564 (2011).
46. B. B. Avants, N. J. Tustison, G. Song, P. A. Cook, A. Klein, J. C. Gee, A reproducible evaluation of ANTs similarity metric performance in brain image registration. *Neuroimage* **54**, 2033–2044 (2011).
47. B. B. Avants, C. L. Epstein, M. Grossman, J. C. Gee, Symmetric diffeomorphic image registration with cross-correlation: Evaluating automated labeling of elderly and neurodegenerative brain. *Med. Image Anal.* **12**, 26–41 (2008).
48. J. Ashburner, J. L. R. Andersson, K. J. Friston, High-dimensional image registration using symmetric priors. *Neuroimage* **9**, 619–628 (1999).
49. J. Ashburner, K. J. Friston, Nonlinear spatial normalization using basis functions. *Hum. Brain Mapp.* **7**, 254–266 (1999).
50. A. D. Leow, I. Yanovsky, M.-C. Chiang, A. D. Lee, A. D. Klunder, A. Lu, J. T. Becker, S. W. Davis, A. W. Toga, P. M. Thompson, Statistical properties of Jacobian maps and the realization of unbiased large-deformation nonlinear image registration. *IEEE Trans. Med. Imaging* **26**, 822–832 (2007).
51. J. F. P. Ullmann, C. Watson, A. L. Janke, N. D. Kurniawan, D. C. Reutens, A segmentation protocol and MRI atlas of the C57BL/6J mouse neocortex. *Neuroimage* **78**, 196–203 (2013).
52. A. L. Janke, J. F. P. Ullmann, Robust methods to create ex vivo minimum deformation atlases for brain mapping. *Methods* **73**, 18–26 (2015).
53. R. W. Cox, AFNI: Software for analysis and visualization of functional magnetic resonance neuroimages. *Comput. Biomed. Res.* **29**, 162–173 (1996).

Acknowledgments: S. Small and U. Khan (Columbia University) are thanked for contributions to some of the data used in these studies. This work was performed at E.E.K.'s 9.4-T Bruker Ascend system at a Columbia University Irving Medical Center site of the Columbia MR Research Center. **Funding:** Funding for this study was provided to K.E.D. by NIH/NINDS R01 NS074874, E.E.K. by NIH 5R01AG038961-10, and the U.K. DRI, which receives its funding from DRI Ltd, funded by the U.K. Medical Research Council, Alzheimer's Society, and Alzheimer's Research UK. **Author contributions:** This study was designed and managed by C.W.F., J.G., E.E.K., and K.E.D. Animal care and breeding was performed by H.Y.F. Mouse MRI acquisition and analysis was performed by C.W.F. and J.G. iDISCO+ immunolabeling data and NeuN$^+$ counting data analyses were performed by H.F. Manuscript preparation was performed by C.W.F., with input from C.W.F., J.G., H.F., E.E.K., and K.E.D. **Competing interests:** K.E.D. is on the board of directors and SAB for Ceracuity LLC. The other authors declare that they have no competing interests. **Data and materials availability:** All data needed to evaluate the conclusions in the paper are present in the paper and/or the Supplementary Materials. The datasets generated during and/or analyzed during the current study are available from the corresponding author upon request.

Submitted 14 May 2020
Accepted 2 September 2020
Published 16 October 2020
10.1126/sciadv.abc8098

Citation: C. W. Fung, J. Guo, H. Fu, H. Y. Figueroa, E. E. Konofagou, K. E. Duff, Atrophy associated with tau pathology precedes overt cell death in a mouse model of progressive tauopathy. *Sci. Adv.* **6**, eabc8098 (2020).